Colloids and Surfaces A: Physicochemical and Engineering Aspects 727 (2025) 138178

Contents lists available at ScienceDirect

Colloids and Surfaces A: Physicochemical and Engineering Aspects

journal homepage: www.elsevier.com/locate/colsurfa

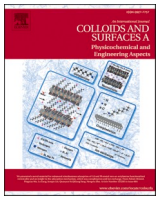

Liquid phase separation of acicular goethite nanoparticles comprising dendrites, intergrowths and hexagonal frames

Monica Distaso [a,b,*], Semanti Banerjee [a]

[a] Interdisciplinary Center for Functional Particle Systems (FPS), Friedrich-Alexander-University Erlangen-Nürnberg (FAU) Haberstraße 9a, Erlangen 91058, Germany
[b] Helmholtz-Institute Erlangen-Nürnberg for Renewable Energy (IET-2), Forschungszentrum Jülich, Cauerstr. 1, Erlangen 91058, Germany

GRAPHICAL ABSTRACT

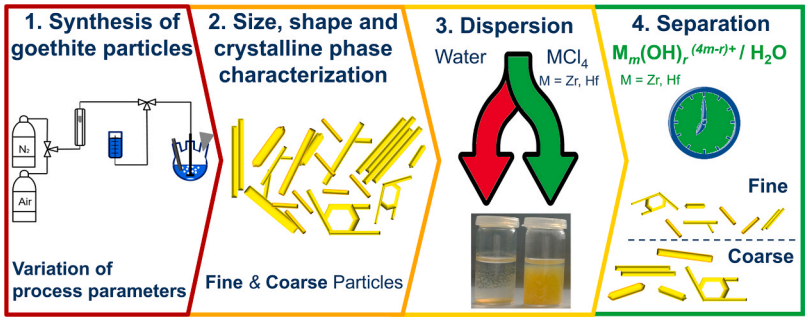

ARTICLE INFO

Keywords:
Colloidal inks
Post-processing
Solid-liquid separation
Colloidal stability

ABSTRACT

The control on the shape and size of nanoparticles is fundamental to control their properties. Besides the design of selective synthetic protocols, the development of size and shape separation methods paves the way towards more homogeneous samples with improved properties. In the current paper, we compare the ability of aqueous solutions of MCl_4 (M = Zr, Hf) to act as colloidal stabilizers for goethite nanoparticles polydisperse in size and shape. More precisely, the occurrence of goethite particles with shapes deviating from the target acicular is ascertain and quantified with respect to experimental conditions during the synthesis. The stabilization method is applied to effectively separate goethite particles into a fine and coarse fraction, which are analysed in depth. Each fraction is characterized by Scanning Electron Microscopy (SEM), electrophoretic mobility to assess Zeta potential and UV-Vis spectroscopy to ascertain the stability of the suspensions and of the separated fractions.

1. Introduction

Functional particles find applications in catalysis and photocatalysis, nanomedicine and cosmetics as well as additives in food, beverages and lubricants [1–3]. In energy related applications, nanoparticles have been exploited in photovoltaic devices, to store energy in batteries and capacitors, and to fabricate sensors [4,5]. In paints and coatings, nanoparticles are key ingredients to enhance properties like durability, water-resistance, antimicrobial activity, and UV protection, or to impart color to substrates and polymeric matrices [6,7]. A global market

* Correspondence to: Helmholtz Institut Erlangen-Nürnberg for Renewable Energy, Cauerstraße 1, 91058 Erlangen, Germany.
E-mail address: m.distaso@fz-juelich.de (M. Distaso).

https://doi.org/10.1016/j.colsurfa.2025.138178
Received 7 July 2025; Received in revised form 14 August 2025; Accepted 24 August 2025
Available online 27 August 2025

volume of 12 million tons was reached in 2020 for the application of inorganic pigments in the field of coatings, paints, printing inks, plastics and cosmetics [8]. In all these applications, it is of outmost importance to ensure control over size, shape and colloidal stability of the materials at hands.

Goethite (α-FeOOH) is an oxyhydroxide material widely used as photocatalyst [9–12] yellow [13] and anti-corrosion pigment [14], absorbent of heavy metals [15–19] and phosphates [20]. More recently, it has been used as anode electrocatalyst in formic acid fuel cells [21]. Finally, goethite is a precursor of acicular magnetite for magnetic recording media [22–24]. In industry, goethite particles are synthesized through ton scale batch precipitation processes based on the hydrolysis of ferrous salts followed by oxidation with air in alkaline environment [25]. The products typically comprise anisotropic particles with acicular shape, and variable amount of particles with anisotropic shapes deviating from the rod-like morphology, such as dendrites, intergrowth and particles with hexagonal frame shape [25]. The presence of such particles in goethite samples is undesired as they interfere with several applications of this material [8,25,26]. Therefore, besides the design of size and shape selective synthetic methods, the development of scalable approaches to separate and classify nanoparticle solids in the liquid phase is considered an important step for further product improvement. Current technologies for particle separation comprise ultracentrifugation, electrophoresis, filtration, chromatography, and selective precipitation carried out in continuous using microfluidic devices [27]. The key requirement for any efficient separation is the colloidal stability.

We have recently demonstrated that goethite particles, among other materials such as ibuprofen and naproxen [28], carbon black based particles and various metal oxide nanoparticles, can be effectively dispersed and stabilized in water using aqueous solutions of Zr(IV) salts [29]. Following our interest for the liquid phase stabilization of functional particles using Zr(IV) hydroxo-complexes as stabilizers, we extend the methodology to the use of aqueous solutions of Hf(IV) as effective stabilizers of goethite particles. We apply our stabilization protocol to separate goethite nanoparticles into a fine and coarse fraction, whereby the latter displays an enrichment in goethite particles deviating from the desired acicular shape [29]. The samples are characterized by X-ray diffraction (XRD) and Scanning Electron Microscopy (SEM), and in liquid phase by Zeta potential and UV-Vis spectroscopy. Our stabilization methodology can be applied to other anisotropic functional materials that crystallize in anisotropic shapes comprising particles deviating from the acicular morphology, such as manganese oxy-hydroxide (MnOOH) and copper oxides (CuO, Cu_2O and Cu_4O_3). Furthermore, the method described herein lays the basis for the deployment of more involved technologies for the solid-liquid separation of particles.

2. Experimental part

All chemicals were commercial sources and have been used without any further purification. $ZrCl_4$ (99.5 %) and $HfCl_4$ (99.9 %) were Alfa Aesar products. NaOH (> 99.0 % purity) was purchased from Carl Roth, and $FeSO_4 \bullet 7H_2O$ (purity > 99.0 %) was a Sigma Aldrich product. Ultrapure water with a resistivity of 18.2 MΩ×cm was deoxygenated by bubbling nitrogen (Linde, 5.0) and used as solvent for the synthesis of goethite particles. Synthetic air (Linde) was used for the oxidation step.

2.1. Synthesis of goethite particles

The synthesis of goethite particles was carried out under alkaline conditions following a protocol described elsewhere [30,31]. In a typical synthesis, an iron sulfate solution with concentration of 0.06 and 0.225 mol/l, was mixed with a sodium hydroxide solution under constant nitrogen bubbling, resulting in a white precipitate of hexagonal platelets of $Fe(OH)_2$. In the former case, the amount of NaOH was adjusted to reach a NaOH/Fe(II) ratio of 6 mol/mol, in the latter case the ratio was kept to 10 mol/mol. Prior to mixing, both solutions were deoxygenated by bubbling nitrogen until the oxygen concentration measured by the immersed oxygen sensor (LnPro6860i/12/420, connected to a multichannel Mettler Toledo transmitter unit, M800) was zero. In the second step, the suspension was oxidized by bubbling air with various rates between 150 and 500 mL/min. The end of oxidation was identified by the steep increase of oxygen concentration in solution, indicating that Fe(II) was completely converted in Fe(III). After reaction, the samples were centrifuged, washed thrice with ultrapure water and dried in oven overnight at 60°C.

2.2. Goethite particles characterization by powder X-ray diffraction (XRD)

X-ray diffraction pattern were measured in Bragg-Brentano geometry using a D8 Advance instrument (Bruker AXS GmbH, Germany) equipped with a Cu Kα radiation. The crystallite size was estimated using the two most intense reflections (110) and the (111) at 21.2 and 36.6 ° using the Scherrer equation and a shape factor 0.9. See Figure S1 in the Supporting Information file.

2.3. Goethite particles characterization by Scanning Electron Microscopy (SEM)

The analysis was performed using an ULTRA 55 microscope (Carl Zeiss AG) at a voltage of 10 keV. Dilute suspensions in water were mild sonicated for several minutes and deposited onto Si/SiO_2 substrates via spin coating or drop casting. The freeware processing software ImageJ (version 1.48r) was used for image analysis and to estimate a representative particle size and shape distribution [32]. To estimate the occurrence of goethite particles with shapes deviating from the acicular morphology, the particles were manually counted from the corresponding electron micrographs whenever isolated particles could be visualized. The manual counting was facilitated upon Zr(IV) stabilization. See Figure S2 in the Supporting Information file, as example of a typical SEM analysis.

2.4. Description of the stabilization protocol

The metal chlorides MCl_4 (M = Zr or Hf) were solubilized in ultrapure water to form a stock solution with typical concentration of 0.04 M. Goethite particles were dispersed in water upon ultrasonication for at least 10 min leading to a stock suspension with typical concentration of 10 mg/mL, 0.113 M. The ultrasonication bath was manufactured by BANDELIN Electronic GmbH & Co, had a nominal power of 215 W and a frequency of 35 kHz. Aliquots of the goethite stock suspension were diluted with ultrapure water and suitable volumes of the freshly prepared aqueous solution of M(IV) stabilizers were added to the goethite suspensions having a concentration of 3.71 mM (0.33 mg/mL). In both cases, no incubation time was necessary to achieve complete dispersion of the solid and stable colloid suspensions. For methodological purposes, the concentration of M(IV) salts was extended to a broad range between 0.0371 mM (for M(IV):Fe = 0.01:1 mol ratio) and 37.1 mM (for M(IV):Fe = 10:1 mol ratio). The reference sample, comprising only goethite particles in water, or in KCl solution for the purpose of electrophoretic measurements, had a pH 6.9, whereas in the presence of the M(IV) stabilizers the pH of the suspensions dropped to acidic values. The higher the concentration of the stabilizer, the lower the pH, until a plateau was reached where the pH did not increase anymore by increasing the concentration of the M(IV) salt. More specifically, for a stabilizer concentration of 0.04 mM, a pH of 5.5 was achieved, which reduces to pH 3 when the concentration of the M(IV) salt increased to 0.4 mM. For M(IV) stabilizer concentrations above the threshold concentration of 0.4 mM, the pH of the suspensions was stable at pH 3. Aliquots of the freshly prepared suspensions were characterized in depth as described in the following section. Alternatively, the suspensions were left to stand still overnight. Afterwards, the supernatant was

carefully separated from the sediment using a pipette. The sediment was redispersed in the same initial volume of deionized water. The supernatant and the redispersed sediment were characterized in liquid phase as described in the following.

2.5. Ultraviolet-visible spectroscopy (UV-Vis)

The extinction of the goethite suspensions were measured using a Varian Cary 100 Scan UV-Visible double-beam spectrophotometer in the wavelength range of 270–800 nm. The optical path was 1 cm. UV-Vis spectroscopy in transmission mode was used to assess the colloidal stability over time. Spectra were acquired every 5 min over a period of 24 h, and 72 h, respectively, for the freshly prepared suspension and for the supernatant after solid-liquid separation, without removing the cuvette from the sample compartment.

2.6. Zeta potential measurements

Electrophoretic mobility were measured by Laser Doppler Electrophoresis using a Zetasizer Nano ZS90 instrument (Malvern Instruments, Malvern, UK) equipped with a 633 nm laser. Zeta potential was calculated using the Henry equation:

$$U_E = 2\varepsilon\zeta f(\kappa a)/3\eta \quad (1)$$

where U_E is the electrophoretic mobility, ζ = Zeta potential, ε the dielectric constant and η is the viscosity of the solvent. $f(\kappa a)$ is the Henry function with κ^{-1} being the Debye length and a referring to the particles size. For experimental conditions investigated in the current work where $\kappa a >> 1$, the electrophoretic mobility of a particle does not depend on its shape and the particle does not rotate in the applied field [33,34]. Therefore, no corrections were applied to take into account the anisotropy of the particles and the ζ-potential was calculated from the mobility measurements using the Smoluchowski model. The electrophoretic mobility increased upon stabilization with aqueous solutions of M(IV) salts with respect to non-stabilized samples, and by increasing the concentration of the salts until a plateau was reached where the mobility was independent of the Zr(IV) or Hf(IV) concentration. The stabilized goethite suspensions were diluted 1:20 (vol: vol) with a water solution of KCl (0.01 M) as background electrolyte prior to measurements.

3. Results and discussion

3.1. Synthesis of goethite particles

Goethite particles are synthesized at industrial scale by precipitation of ferrous salts under alkaline environment followed by air oxidation. Typically, $FeSO_4$ is used as starting salt which is obtained by dissolution of iron scraps in sulphuric acid [25]. Moreover, $FeSO_4$ is an abundant source of iron, as it is a by- product in the production of TiO_2 nanoparticles through the sulphate process involving the mineral Ilmenite [35,36]. The solution is then mixed with NaOH in water, and the obtained slurry undergoes oxidation to Fe(III) using air as oxidizing agent [25].

At laboratory scale, the mixing step between the Fe(II) and the NaOH solutions can be easily carried out under anaerobic conditions, leading to the formation of hexagonal discs of $Fe(OH)_2$ [25,30]. Subsequently, different aeration flow rates enable the tuning of particle size distributions [30,31]. The Scanning Electron Microscopy (SEM) analysis of a typical goethite sample shows the presence of mainly acicular particles often bundled in large agglomerates with sizes of several micron (Fig. 1a). Additionally, particles deviating from the acicular morphology such as dendrites, intergrowth, and hollow/hexagonal frames are easily identified in SEM micrographs (Fig. 1b)–d)), as well as in Transmission Electron Microscopy (TEM) images (Fig. 1f) and g)). These objects result from the complex formation mechanism of goethite nanoparticles. A widely observed deviation of goethite particle shapes from acicular morphology are hollow particles with a hexagonal frame (Fig. 1b), c) and g)). We have shown that this particle morphology arises from the epitaxial growth of goethite on the edges of $Fe(OH)_2$ hexagons formed in the first synthesis step under anaerobic conditions. After the dissolution of $Fe(OH)_2$ a hollow goethite particle is formed [30]. Additional particles deviating from acicular shape are observed via SEM analysis. Dendrites are particles with lateral branches that develop from the c- axis of acicular goethite with an angle of ca. 117 ° due to the formation of twins between the (020) and the (021) planes [25]. An example of goethite

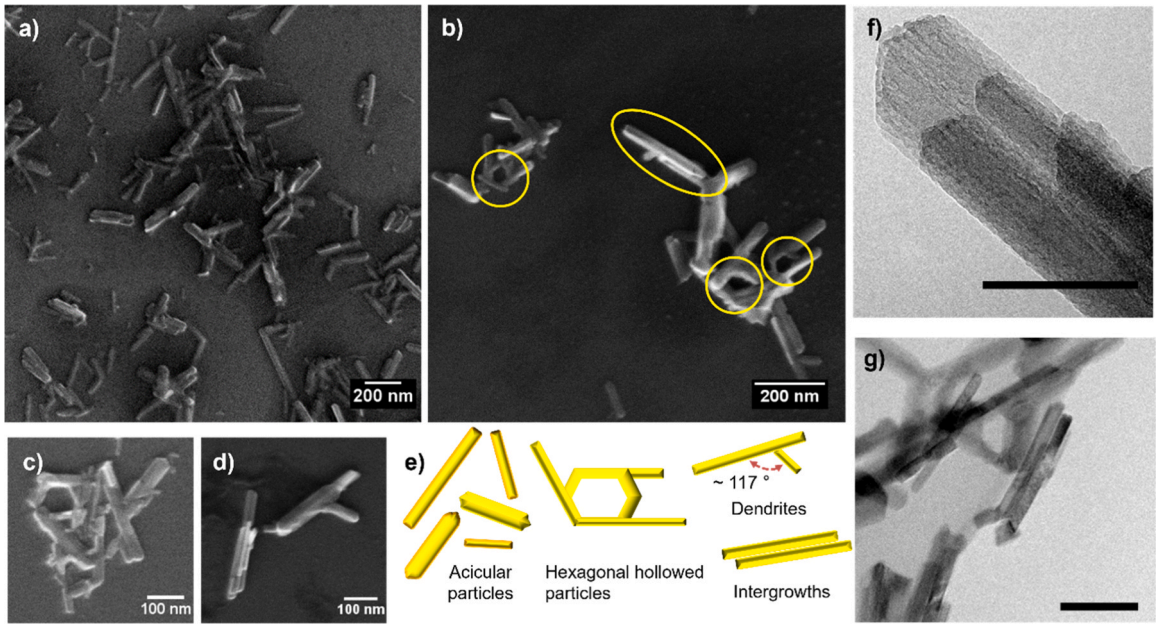

Fig. 1. Electron microscopy characterization of a typical goethite sample obtained by precipitation of $Fe(SO_4)\cdot 7H_2O$ with NaOH in water followed by oxidation with oxygen. Scanning Electron Microscopy (SEM) images in Figure a)-d). a) Overview of the sample; b) and c) close-up image on hollowed particles; d) close-up on intergrowths (on the left) and a dendrite particle (on the right); e) schematic of the shape composition of the sample. Transmission Electron Microscopy (TEM) images in Figure f) and g). f) Intergrowth; g) hexagonal frames and intergrowths. The scale bar in TEM images is 50 nm.

dendrites isolated under our experimental conditions is shown in Fig. 1d (right). Finally, several goethite rods are often aligned along the *c*-axis and stacked along the *a*- and *b*- axis, leading to domains of intergrowths (Fig. 1d left, and 1 f)) [25]. It has been shown in the literature that intergrowth are intermediates in the crystallization of goethite acicular particles by oriented attachment [31,37].

The occurrence of dendrite formation for goethite has been reported as well by other authors upon use of cetyltrimethylammonium bromide (CTAB) and gum arabic (GA) as organic ligand modulators [38]. Qasim et al. have demonstrated that goethite intergrowths are efficient photocatalysts for water oxidation [39].

The formation of dendrites is a widespread phenomenon in geological deposits and minerals [40,41], urban environment [42], and human artifacts [43]. Dendrites form during the electrodeposition of copper oxide films (Cu_2O, CuO and Cu_4O_3) [44], and the formation of MnOOH dendritic nanorods under hydrothermal conditions [45,46]. The occurrence of dendrites in functional materials is not always detrimental. For example, Tian et al. have demonstrated that hierarchical dendrite-like structures of iron layered double hydroxide are effective in the removal of arsenic from waste water [47]. However, for goethite particles the occurrence of dendrites is particularly undesired as they hinder the applicability of goethite particles as precursor of maghemite and magnetite in magnetic recording devices [26].

Herein for the specific case of goethite particles, we show that the number of particles deviating from acicular morphology highly depends on the experimental conditions used for the synthesis of goethite nanoparticles. Besides the mixing intensity between $FeSO_4$ and NaOH solutions, the absolute concentrations of Fe(II) and NaOH and the NaOH/Fe(II) molar ratio, the aeration rate are crucial experimental parameters. In general, higher concentration of Fe(II) favours the formation of larger particles, both in length and width.

To understand the impact of the aeration rate on the occurrence of anisotropic shapes deviating from the acicular morphology, the initial concentration of $FeSO_4$ was kept constant at 0.06 M, and the NaOH/Fe (II) molar ratio was fixed to 6 to control the pH and enable the solely formation of goethite phase upon aeration. Then, the aeration rate was increased from 150 mL/min to 500 mL/min. An in-depth analysis of the SEM images of the as-obtained goethite particles allows to quantify the occurrence of the different particle shapes.

Fig. 2 shows that by increasing the aeration rate, the percentage of particles with shapes deviating from acicular morphology increases too. Herein, the intergrowths are considered within the class of dendrites, following the electron microscopy characterization of Rösler et al [26].

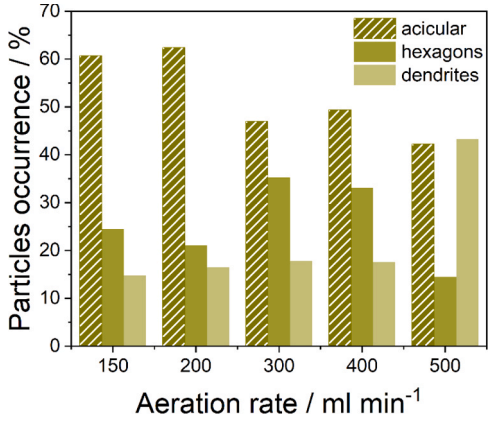

Fig. 2. Statistical evaluation of SEM micrographs to estimate the number of goethite particles deviating from acicular shape as function of the aeration rate during the synthesis. The total number of particles evaluated for each sample was: 257 (150 mL/min); 484 (mL/min); 315 (300 mL/min); 387 (400 mL/min) and 400 (500 mL/min). The experimental conditions for the synthesis comprised: $[FeSO_4] = 0.06$ M; $[NaOH]/[Fe(II)] = 6$; T = 35 °C [30].

To the best of our knowledge, this is the first time that the occurrence of dendrites, intergrowth and particles with hexagonal shapes is quantified as function of the experimental parameters. Fig. 3 shows that in the aeration rate interval considered in the current work, the size of the particles is broadly distributed independent of their shapes. In particular, the mean lengths of the acicular goethite particles, the lateral branch of the dendrites and the length of the rods included in the intergrowth are very similar (Fig. 3a). Considering the hexagonal frames, they were approximated to full particles in order to measure the corresponding Feret's diameter (Experimental part). The size distributions of the hexagonal frames through the various samples show median size $x_{50,0}$ around 35 nm, with broad spans ($x_{5,0}$ and $x_{95,0}$) of the cumulative distribution, independent of the aeration rate (Fig. 3b). The crystallinity of the samples was assessed by applying the Scherrer equation (shape factor 0.9) to the reflection (110) and (111) at around 21.2 and 36.6 2θ°, respectively, of the powder diffraction pattern (Figure S1 and S2 in Supporting Information).

The results show that the coherence length was also very similar in between the samples, and independent of the aeration rate between 150 mL/min and 500 mL/min (Fig. 3b). Therefore, the aeration rate between 150 and 500 mL/min leads to crystalline goethite particles broadly distributed in size and shapes. The change in particle shape with aeration rate can be related to the increased oxygen mass transfer to the liquid phase at increasing air flow rates. This leads to a faster formation of Fe(III) species generated by oxidation of Fe(II) and in turns to a faster growth with reduced shape selectivity [30,31].

3.2. Water chemistry of Zr(IV) and Hf(IV) ions

Before moving to the first step of our study, involving the transfer of solid goethite particles in water, it is worth to trace a short overview of the water chemistry of Zr(IV) and Hf(IV) [29]. As Lewis acids, zirconium and hafnium salts readily undergo hydrolysis according to the following chemical equilibrium (Eq. (3)):

$$m\mathrm{M}^{4+} + 2r\mathrm{H_2O} \Leftrightarrow \mathbf{M}_m\mathbf{(OH)}_r^{(4m-r)+} + r\mathrm{H_3O}^+ \quad (3)$$

where M = Zr, Hf. The chemistry of these two elements is very similar [48]. When M = Zr, the hydroxo complexes formed in Eq. (3) can be either mononuclear (m = 1) or polynuclear (m ≥ 2) according to the pH and the initial salt concentration [48]. Polynuclear complexes of Zr(IV) form below pH 2 by olation of OH groups [48,49]. The binuclear complex of Zr(IV), was reported for the first time in 1966 [50], and the tetramer species $[Zr_4(OH)_8(OH_2)_{16}]^{8+}$ was obtained by evaporation of aqueous solution of $ZrCl_4$ with acetate as counterion [51]. $Zr(OH)_4$, $Zr(OH)_3^+$, and $Zr(OH)_2^{2+}$ have been predicted to be the most abundant species in pH intervals between 3 and 2.75, between 2.75 and 2.0, and between 2.0 and 1.0, respectively [52]. Concerning Hf(IV), Rai et al. reported that $Hf(OH)_3^+$ complexes are present at pH < 2, whereas $Hf(OH)_5^-$ is the most abundant species between pH 4 and 8, and $Hf(OH)_6^{2-}$ are present at pH above 8 [53]. Polynuclear complexes of Hf(IV) are also well known in the literature, with m = 9 [54], 11 [55] and 18 (Eq. (3)) [56]. Polynuclear complexes of both Zr(IV) and Hf(IV) have been isolated as prenucleation clusters and identified as intermediates in the hydrothermal synthesis of ZrO_2 and HfO_2, respectively [57]. The threshold between mononuclear and polynuclear complexes for both metals is 10^{-4} M, and pH above 0 [58]. It is important to mention here that the mean bond distance of Hf−O both in mononuclear complexes, and in the tetramers (m = 4, Eq. (3)) is shorter than the corresponding values for Zr−O species [58], leading, for example, to smaller unit cells for the polynuclear complexes of Hf(IV) with m = 17 (Eq. (3)) [57]. In aqueous solution, the hydrated Zr(IV) and Hf(IV) ions are eight-coordinated in square antiprismatic geometry, with mean Zr–O and Hf–O bond distances of 2.187 and 2.160 Å, respectively [58]. In the tetramer complex, the mean values of the Zr−O bond is 2.140 Å, and Hf−O is 2.110 Å. The ionic radius of Hf(IV) is smaller than the ionic

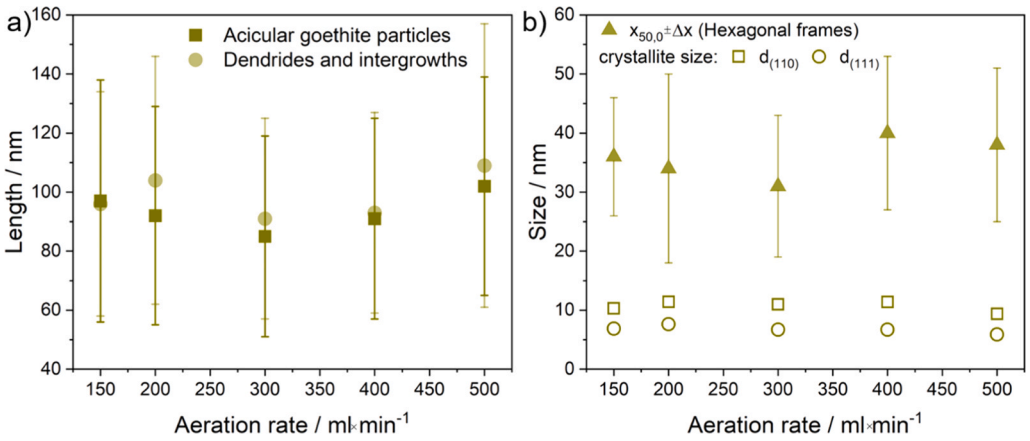

Fig. 3. Assessment and comparison of the goethite particles descriptors as function of the aeration rates. a) Mean length and standard deviation of the acicular particles compared with the branch of dendrites and length of intergrowths; b) median size of the hexagonal frames and coherence length for the (110) and (111) reflections, estimated through the Scherrer equation (shape factor 0.9).

radius of Zr(IV), due to relativistic effects and to the larger effective nuclear charge due to smaller shielding [58].

While it is difficult to assign the exact nature of the Zr- and Hf-hydroxo complexes formed in water, we have demonstrated the effectiveness of Zr(IV) aqueous solution to act as stabilizers of both organic and inorganic species comprising carboxylic and OH groups [28,29]. Accordingly, various nonsteroidal anti-inflammatory drugs (Ibuprofen, Indomethacin, Naproxen and Mefenamic acid) could be effectively stabilized in nanoparticulate form by exploiting the reactivity of the Zr(IV) complexes with the carboxylic acid groups [28]. Moreover, Zr(IV) hydroxo-complexes effectively stabilize a broad range of metal oxide nanoparticles such as TiO_2, CeO_2, SnO_2, V_2O_5, and goethite, enabling their liquid phase characterization [29]. In particular, for goethite nanoparticles it has been demonstrated that the mechanism of stabilization implies a direct interaction of the Zr(IV) complexes with the surface stoichiometric OH groups, leading to a strong adsorption ($\Delta H = -70 \pm 25$ kJ/mol) of the Zr(IV) salts onto the surface of goethite. Such interaction induces excellent colloidal stability and enables the in-depth liquid phase analysis of the goethite particles. Considering the similar chemistry between Zr(IV) and Hf(IV), it was interesting for us to first explore whether our stabilization method could work also with Hf(IV), and afterwards to compare the effectiveness of the two salts in the liquid phase separation of a size- and shape- polydisperse goethite sample.

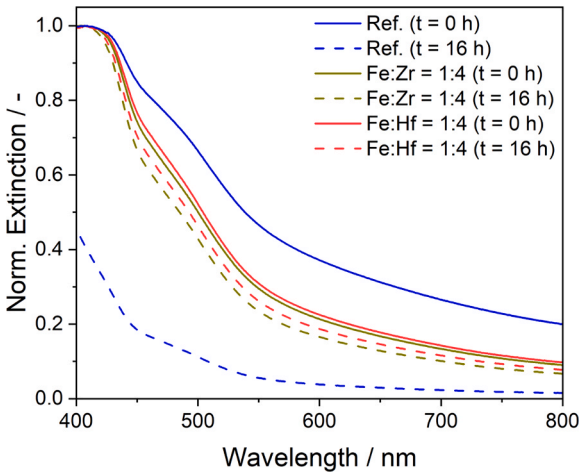

Fig. 4. Optical properties of non-stabilized and M(IV) stabilized goethite NPs suspensions with concentration of 3.714 mM (0.33 mg/mL). The suspensions were diluted (1–15) to reach a maximum of extinction below 1 a.u. at all wavelength. The concentration of M(IV) salts in the diluted suspensions was 0.001 M. The spectra were normalized to the extinction of the reference sample at time 0.

3.3. Dispersion of goethite nanoparticles in aqueous solution of M(IV) complexes (M = Zr, Hf)

In the presence of an aqueous solutions of Zr(IV) or Hf(IV), goethite nanoparticle powders are easily dispersed resulting in stable colloid suspensions. Fig. 4 shows the UV-Vis spectra of goethite particles in water with and without stabilizers, whereby the extinction of goethite particles dispersed in water is remarkably reduced in the presence of water solutions of $ZrCl_4$ or $HfCl_4$. As the concentration of goethite particles is constant, the reduction of the extinction at longer wavelengths can be correlated with the reduction of the size of the agglomerates of rods that are present in the suspensions. In fact, according to theory, for wavelengths longer than 550 nm the extinction of goethite is dominated by scattering and the larger the size of the particles or agglomerates, the larger the extinction, i.e. the scattering, respectively [59–61]. Therefore, the decrease of the extinction observed in the stabilized suspensions, suggests that the stabilization implies a disentanglement of primary particles leading to a reduction of the size of the agglomerates in suspension and consequently, of the scattering at longer wavelengths (Fig. 4, *cf.* solid blue-, green and red lines, for the reference, the Zr(IV) and the Hf(IV) stabilizers, respectively).

The stability of the suspensions with MCl_4 (M = Zr, Hf) molar concentration of 0.001 M was followed over time via UV-Vis spectroscopy at 25 °C and compared with a non-stabilized sample of goethite particles dispersed in water upon ultrasonication. Fig. 4 shows that the extinction of the reference suspension is reduced by more than 80 % at 450 nm and by more than 90 % at 800 nm after 16 h, whereas the M(IV) stabilized suspension shows, after the same time, a reduction of the extinction of only about 10 % at 450 nm (Fig. 4, *cf.* dashed blue, green and red lines, for the reference, the Zr(IV) and the Hf(IV) stabilizers, respectively). The aqueous solution of Hf(IV) seems to be more effective stabilizers than the corresponding Zr(IV) solutions, although both salts show similar stabilization ability for goethite. Additionally, these results suggest that there is a fraction of the particles that sediments during the first 16 h, leaving in the liquid phase a much more stable fraction of particles. While it is expected that larger particles would sediment, it was interesting to shed light on the sedimentation behavior of goethite particles with anisotropic shape, in particular with respect to those deviating from the acicular morphology (Figs. 1–3).

Therefore, a solid-liquid separation step was carried out to separate the supernatant from the particles that sediment after 16 h, and each

fraction was characterized in depth. For these experiments goethite nanorods with mean length and width size of (375 ± 125) nm and (35 ± 10) nm, respectively, were used. These particles were synthesized using a $FeSO_4$ concentration of 0.225 M, a NaOH/Fe(II) ratio of 10 and an aeration rate of 500 mL/min [31]. For such sample, the assessment of the shape distribution showed the presence of around 60 % acicular particles and 40 % of other shapes (Fig. 3c).

Goethite suspensions with MCl_4 (M = Zr, Hf) concentrations between 0.0371 mM and 33 mM were left to sediment by gravity at room temperature for 16 h. Afterwards, the supernatant was pipetted and the sediment was re-dispersed in the same water volume. The supernatant, the re-dispersed sediment in water and the as-prepared stabilized suspensions were analyzed by UV-Vis spectroscopy and the electrophoretic mobility was measured to assess the Zeta potential.

UV-Vis spectroscopy of the fractionated samples showed that the sediments possess also stronger extinction, i.e. scattering (vide supra) at wavelengths longer than 550 nm for both stabilizers (Fig. 5a and b).

The Zeta potential was measured for the full sample, separated supernatant and re-dispersed sediment for both stabilizers (Fig. 6). For the Zr(IV)-stabilized suspension, the high Zeta potential measured for the separated supernatant and full sample indicates a very high colloidal stability. The Zeta potential measurements of the re-dispersed sediments show that the values are remarkably smaller than the corresponding full sample and removed supernatant, respectively. These differences are more pronounced for Zr(IV) concentrations lower than 0.75 mM (Fig. 6a). We have attributed this behavior to the incomplete coverage of the surface for the larger particles in the sediment. A pure dilution effect of the total Zr(IV) content in the redispersed sediment, could be excluded for lower concentrations because, as mentioned above, the interaction of Zr(IV) with the surface of goethite particles is very strong with a ΔH_{ads} = -70 kJ/mol measured by Isothermal Titration Calorimetry, ITC [28]. Though, a dilution effect could be responsible for the slightly lower values of the Zeta potential on the plateau, once the surface of the sedimented particles is also completely covered. This is understandable considering that along the [001] direction, anisotropic goethite nanoparticles, independent of their specific shape, comprise exposed OH stoichiometric groups that are available for the interaction with Zr(IV) or Hf(IV) hydroxo-complexes [26,28,61]. Therefore, the larger the particles, the higher the number of OH groups available and the higher the concentration of Zr(IV) required to achieve a complete coverage of the goethite particles in the coarse fraction.

Moving to the aqueous solution of Hf(IV) complexes, the mean apparent Zeta potential of the sediment redispersed in water shows values very similar to those measured for the full suspension and for the supernatant, respectively (Fig. 6b). This result suggests that a lower concentration of $HfCl_4$ is required to reach Zeta potential values at the plateau for $ZrCl_4$, indicating that Hf(IV) is a better stabilizer than Zr(IV) at the same molar concentration. In fact, at the same Zr(IV) concentration, the Hf(IV) hydroxo- complexes provide a better stabilization also for the sediment. The $ZrCl_4$ threshold concentration is around 0.75 mM, whereas for the $HfCl_4$, the threshold concentration to achieve stable Zeta potential values is much lower at around 0.2 mM.

A possible explanation is provided by our previous discussion about the chemistry of Zr(IV) and Hf(IV) ions. These two elements have a very similar chemistry, however, the Hf(IV) hydroxo-complexes, either as mononuclear or polynuclear species, are smaller than the corresponding Zr(IV) complexes [58]. Herein, it is proposed that the smaller size of Hf (IV) complexes enable a more effective adsorption onto the surface of goethite particles. Additionally, their smaller size leads to a higher charge density, which is also a parameter that can affect the colloidal stabilization. While aqueous solutions of the MCl_4 salts can be used indifferently for the stabilization of suspensions, for the purpose of solid-liquid separation and in light of a possible large scale application, the use of Zr(IV) species at lower concentration should be preferred based on its relative abundancy. Additionally, hafnium is classified as a critical raw material by the European Community [62]. Therefore, the subsequent statistical analysis was carried out on the sediment separated from the Zr(IV) stabilized suspension, also considering the less effective colloidal stabilization of the sediment for Zr(IV) concentration lower than 0.75 mM. Accordingly, the supernatant and the sediment for the goethite sample stabilized with 0.75 mM Zr(IV) aqueous solutions were analyzed by SEM and the occurrence of acicular particles, and of particles deviating from the acicular morphology was assessed by manual counting the particles from the corresponding electron micrographs. The results show that the re-dispersed sediment is enriched in particles deviating from the acicular shape (Fig. 6c). In particular, it was observed that goethite particles with other morphologies were around 30 % in the supernatant and increased to 45 % in the sediment. These data indicates that the sediment is enriched with particles deviating from the acicular shape (Fig. 6c). After separation, the stability of the supernatant was monitored for additional 70 h by UV-Vis spectroscopy, showing an excellent stability (Fig. 6d).

Taken together, the results show that the goethite particles that sediment under gravity after 16 h have higher scattering in the visible and a lower Zeta potential than the particles remaining in suspensions for lower Zr(IV) (Figs. 5 and 6a). This fraction is enriched in goethite particles with non-acicular shape (Fig. 6b). On the other side, the particles that remain in the supernatant, have lower scattering in the visible and higher Zeta potential (Fig. 6c). Therefore, the colloidal stabilization of goethite particles using aqueous solutions of Zr(IV) complexes has enabled a separation between the fine and coarse fraction of a size and shape polydispersed goethite sample. The aqueous solutions of $HfCl_4$ are more effective stabilizers than the corresponding solution of $ZrCl_4$. To the best of our knowledge, this is the first time that the separation of goethite particles with shapes deviating from acicular morphology is attempted.

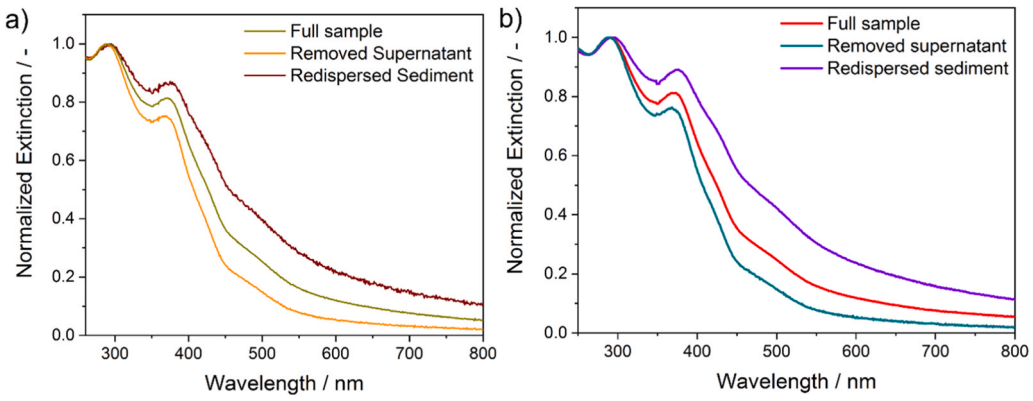

Fig. 5. UV-Vis spectra of the full suspensions, removed supernatants and re-dispersed sediments after 16 h at room temperature for aqueous solutions of: a) $ZrCl_4$ and b) $HfCl_4$. Rods with mean length and width size of (375 ± 125) nm, and (35 ± 10) nm, respectively were used.

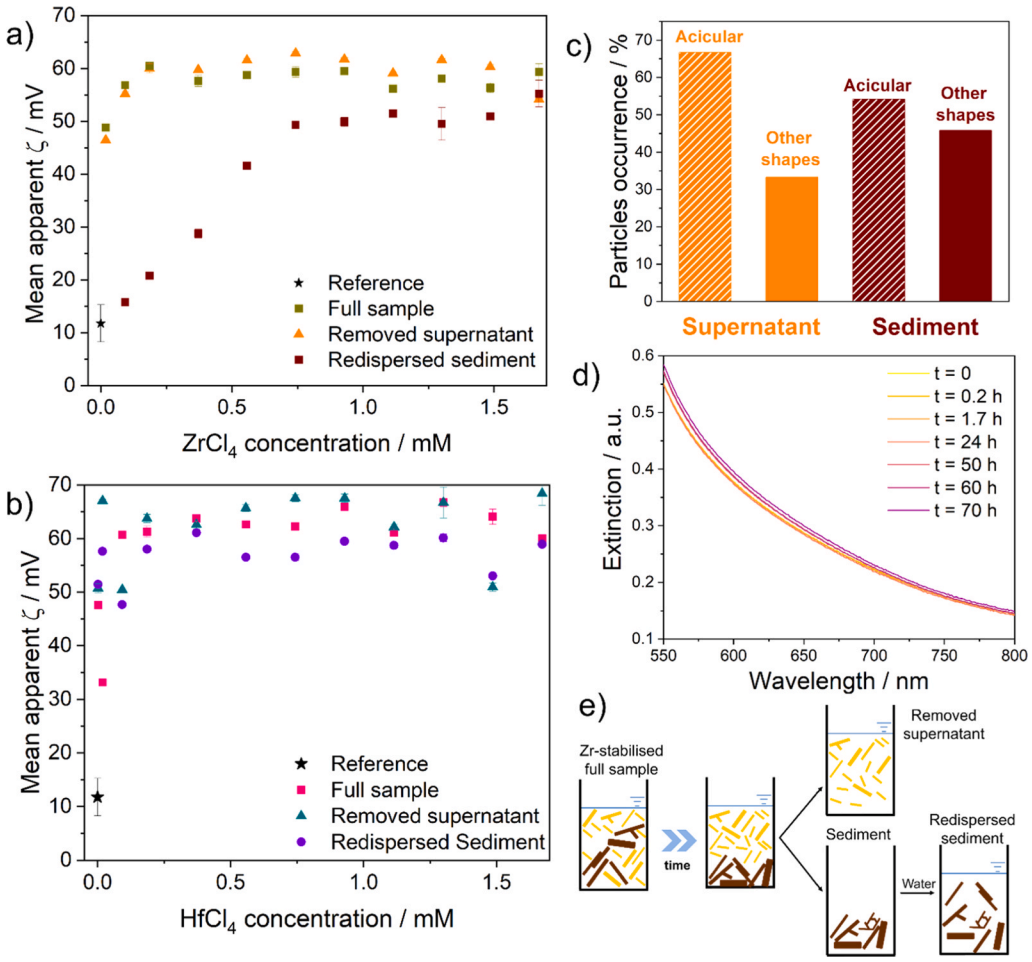

Fig. 6. a) Zeta potential of the full suspensions, removed supernatants and redispersed sediments after 16 h at room temperature for different $ZrCl_4$ concentrations compared with a non-stabilized goethite sample taken as reference. b) Zeta potential of the full suspensions, removed supernatants and redispersed sediments after 16 h at room temperature for different $HfCl_4$ concentrations compared with a non-stabilized goethite sample taken as reference. All suspensions, including the reference, were diluted with a 0.01 M KCl solution to ensure the same bulk ionic strength throughout the samples. c) Statistical evaluation of SEM micrographs to estimate the number of goethite particles deviating from acicular shape in a stabilized goethite sample ($[ZrCl_4] = 0.75$ mM) upon solid-liquid separation. The total number of particles evaluated for each sample was: 1005 for the supernatant and 463 for the sediment. d) Extinction at the specified time in the spectral range between 550 nm and 800 nm after the separation of the coarse fraction. $[FeSO_4] = 0.225$ M; $[NaOH]/[Fe(II)] = 10$; aeration rate = 500 mL/min; T = 35 °C [31]. e) Schematic of the solid-liquid separation approach.

4. Conclusions

In the current paper, we have compared the ability of aqueous solutions of MCl_4 (M = Zr, Hf) to act as stabilizers for size and shape polydisperse samples of goethite nanoparticles. More precisely, we have exploited the ability of M(IV) hydroxo-complexes to separate goethite particles into fine and coarse fractions. While both Zr(IV) and Hf(IV) aqueous solutions act as effective stabilizers of goethite particles, using the cheaper and more abundant Zr(IV) salt, the supernatant has been demonstrated to be stable in solution for more than 70 h, proving a remarkable long-term colloidal stability. The sediment has shown an enrichment of anisotropic particles with shapes deviating from the acicular morphology. The resulting supernatant fraction presents improved material properties, such as reduced scattering in the visible due to the absence of aggregates, and increased colloidal stability indicated by the higher Zeta potential, and stable extinction values for more than 70 h. The method proposed herein is an effective strategy to analyze in depth complex nanoparticulate products comprising broad size and shape distribution through a combination of solid- and liquid phase analytical techniques. In particular, the sedimentation by gravity may serve as a straightforward tool to low-cost, and energy-efficient separation of particles in a suspension based on their size and density. The approach developed in the current work can be applied to the size and shape separation of other material systems comprising OH groups and shapes deviating from the acicular shape, such as dendritic MnOOH and copper oxides (Cu_2O, CuO, Cu_4O_3). The longtime stability of the supernatant after separation of the coarse fraction enables the use of the corresponding nanoparticulate suspension as printable inks.

CRediT authorship contribution statement

Semanti Banerjee: Writing – review & editing, Validation, Methodology. **Monica Distaso:** Writing – review & editing, Writing – original draft, Validation, Supervision, Methodology, Investigation, Formal analysis, Data curation, Conceptualization.

Conflict of interest

The authors declare no conflict of interest.

Acknowledgments

The authors acknowledge funding from the Deutsche Forschungsgemeinschaft (DFG) through the Cluster of Excellence

Engineering of Advanced Materials at FAU Erlangen-Nürnberg.

Appendix A. Supporting information

Supplementary data associated with this article can be found in the online version at doi:10.1016/j.colsurfa.2025.138178.

Data availability

Data will be made available on request.

References

[1] M.A. Hassaan, M.A. El-Nemr, M.R. Elkatory, S. Ragab, V.-C. Niculescu, A. El Nemr, Top. Curr. Chem. (Cham) 381 (2023) 31.
[2] J. Chen, Y. Guo, X. Zhang, J. Liu, P. Gong, Z. Su, L. Fan, G. Li, J. Agric. Food Chem. 71 (2023) 3564–3582.
[3] S. Shahnazar, S. Bagheri, S.B. Abd Hamid, Int. J. Hydrogen Energy 41 (2016) 3153–3170.
[4] S. Kundu, A. Patra, Chem. Rev. 117 (2017) 712–757.
[5] Y. Ma, X. Xie, W. Yang, Z. Yu, X. Sun, Y. Zhang, X. Yang, H. Kimura, C. Hou, Z. Guo, W. Du, Adv. Compos. Hybrid. Mater. 4 (2021) 906–924.
[6] M.C. Chen, P.W. Koh, V.K. Ponnusamy, S.L. Lee, Prog. Org. Coat. 163 (2022) 106660.
[7] G. Pfaff, Inorganic Pigments, De Gruyter, Berlin, Boston, 2017.
[8] G. Pfaff, ChemTexts 8 (2022).
[9] S. Kakuta, T. Numata, T. Okayama, Catal. Sci. Technol. 4 (2014) 164–169.
[10] A.C. Kuncser, I.D. Vlaicu, O.D. Pavel, R. Zavoianu, M. Badea, D. Radu, D.C. Culita, A.M. Rostas, R. Olar, RSC Adv. 11 (2021) 27589–27602.
[11] B. Xu, X. Dai, Q. Tan, Y. Wei, G. Liu, G. Wu, CrystEngComm 22 (2020) 2827–2836.
[12] H. Pan, K.R. Martindale, M.D. Heagy, Top. Catal. 61 (2018) 601–609.
[13] M. Müller, J.C. Villalba, F.Q. Mariani, M. Dalpasquale, M.Z. Lemos, M.F. Gonzalez Huila, F.J. Anaissi, Dyes Pigments 120 (2015) 271–278.
[14] Y. Touazi, A. Abdi, A. Leshaf, K. Khimeche, Prog. Org. Coat. 139 (2020) 105458.
[15] L. Newsome, K. Morris, A. Cleary, N.K. Masters-Waage, C. Boothman, N. Joshi, N. Atherton, J.R. Lloyd, J. Hazard. Mater. 364 (2019) 134–142.
[16] E. Chmielewská, W. Tylus, M. Drábik, J. Majzlan, J. Kravčak, C. Williams, M. Čaplovičová, Ľ. Čaplovič, Microporous Mesoporous Mater. 248 (2017) 222–233.
[17] A.K. Patra, D. Kim, ACS Sustain. Chem. Eng. 5 (2017) 1272–1279.
[18] J. He, F. Bardelli, A. Gehin, E. Silvester, L. Charlet, Water Res. 101 (2016) 1–9.
[19] M. Mohapatra, K. Rout, S.K. Gupta, P. Singh, S. Anand, B.K. Mishra, J. Nanopart. Res 12 (2010) 681–686.
[20] M.T. Spicher, S.P. Schwaminger, D. von der Haar-Leistl, M. Reindl, F.E. Wagner, S. Berensmeier, J. Colloid Interface Sci. 634 (2023) 418–430.
[21] B.A. Al-Qodami, H.H. Alalawy, I.M. Al-Akraa, S.Y. Sayed, N.K. Allam, A. M. Mohammad, Int. J. Hydrogen Energy 47 (2022) 264–275.
[22] S. Laurent, D. Forge, M. Port, A. Roch, C. Robic, L. Vander Elst, R.N. Muller, Chem. Rev. 108 (2008) 2064–2110.
[23] R. Mariño-Fernández, S.H. Masunaga, N. Fontaíña-Troitiño, M.P. Morales, J. Rivas, V. Salgueirino, J. Phys. Chem. C 115 (2011) 13991–13999.
[24] C. Sudakar, G.N. Subbanna, T.R.N. Kutty, J. Mater. Sci. 39 (2004) 4271–4286.
[25] R.M. Cornell, U. Schwertmann, The Iron Oxides. Structure, Properties, Reactions, Occurences and Uses, Wiley-VCH GmbH & Co. KGaA, Weinheim, 2003.
[26] M. Rösler, H. Hofmeister, E. Held, in: P. Jena, S.N. Khanna, B.K. Rao (Eds.), Physics and Chemistry of Finite Systems: From Clusters to Crystals, Springer Netherlands, Dordrecht, s.l., 1992, pp. 111–118.
[27] T. Salafi, K.K. Zeming, Y. Zhang, Lab a Chip 17 (2016) 11–33.
[28] H. Trzenschiok, M. Distaso, W. Peukert, Chem. Eng. J. 361 (2019) 428–438.
[29] M. Distaso, V. Lautenbach, M.J. Uttinger, J. Walter, C. Lübbert, T. Thajudeen, W. Peukert, Powder Technol. 407 (2022) 117633.
[30] E.R. Encina, M. Distaso, R.N. Klupp Taylor, W. Peukert, Cryst. Growth Des. 15 (2014) 194–203.
[31] A. Güldenpfennig, M. Distaso, R.N. Klupp Taylor, W. Peukert, Chem. Eng. J. 347 (2018) 798–807.
[32] W.S. Rasband, ImageJ, U.S. National Institutes of Health.
[33] F. Morrison, J. Colloid Interface Sci. 34 (1970) 210–214.
[34] H.E. Bakker, T.H. Besseling, J.E.G.J. Wijnhoven, P.H. Helfferich, A. van Blaaderen, A. Imhof, Langmuir ACS J. Surf. Colloids 33 (2017) 881–890.
[35] S. Grant, A.A. Freer, J.M. Winfield, C. Gray, T.L. Overton, D. Lennon, Green Chem. 6 (2004) 25.
[36] N.A. Ramos-Delgado, M.Á. Gracia-Pinilla, R.V. Mangalaraja, K. O'Shea, D. D. Dionysiou, Nanotechnol. Rev. 5 (2016) 467–479.
[37] H. Yang, X. Zhou, T. Tang, X. Qi, C. Wang, J. Lan, Y. Wang, Y. Yang, G. Liu, CrystEngComm 12 (2010) 4007.
[38] M. Ristić, I. Opačak, J. Štajdohar, S. Musić, J. Mol. Struct. 1090 (2015) 129–137.
[39] M. Qasim, F. Xue, M. Liu, L. Guo, J. Photon. Energy 9 (2019) 1.
[40] B. Chopard, H.J. Herrmann, T. Vicsek, Nature 353 (1991) 409–412.
[41] H. Xu, T. Chen, H. Konishi, Am. Mineral. 95 (2010) 556–562.
[42] E.P. Vicenzi, C.A. Grissom, R.A. Livingston, Z. Weldon-Yochim, Herit. Sci. 4 (2016).
[43] C.-Y. Chiang, H.F. Greer, R.-S. Liu, W. Zhou, Ceram. Int. 42 (2016) 7506–7513.
[44] Z. Mezine, A. Kadri, L. Hamadou, N. Benbrahim, A. Chaouchi, J. Electroanal. Chem. 817 (2018) 36–47.
[45] Y.X. Zhang, M. Dong, S.J. Zhu, C.P. Liu, Z.Q. Wen, Physica B Condensed Matter 416 (2013) 23–28.
[46] Y. Li, H. Tan, O. Lebedev, J. Verbeeck, E. Biermans, G. van Tendeloo, B.-L. Su, Cryst. Growth Des. 10 (2010) 2969–2976.
[47] N. Tian, X. Tian, X. Liu, Z. Zhou, C. Yang, L. Ma, C. Tian, Y. Li, Y. Wang, Chem. Commun. (Camb. Engl.) 52 (2016) 11955–11958.
[48] P.L. Brown, C. Ekberg, Hydrolysis of Metal Ions, Wiley-VCH Verlag GmbH & Co. KGaA, Weinheim, Germany, 2016.
[49] P.D. Southon, J.R. Bartlett, J.L. Woolfrey, B. Ben-Nissan, Chem. Mater. 14 (2002) 4313–4319.
[50] D.B. McWhan, G. Lundgren, Inorg. Chem. 5 (1966) 284–289.
[51] C. Hennig, S. Weiss, W. Kraus, J. Kretzschmar, A.C. Scheinost, Inorg. Chem. 56 (2017) 2473–2480.
[52] C. Eckberg, G. Källvenius, Y. Albinsson, P.L. Brown, J. Solut. Chem. 33 (2004) 47–79.
[53] D. Rai, A. Kitamura, M. Altmaier, K.M. Rosso, T. Sasaki, T. Kobayashi, J. Solut. Chem. 47 (2018) 855–891.
[54] A. Kalaji, L. Soderholm, Chem. Commun. (Camb. Engl.) 50 (2014) 997–999.
[55] A. Kalaji, L. Soderholm, Inorg. Chem. 53 (2014) 11252–11260.
[56] W. Mark, M. Hansson, Acta Crystallogr. B Struct. Sci. 31 (1975) 1101–1108.
[57] Q. Sun, C. Liu, G. Zhang, J. Zhang, C.-H. Tung, Y. Wang, Chem. (Weinh. der Bergstr. Ger.) 24 (2018) 14701–14706.
[58] C. Hagfeldt, V. Kessler, I. Persson, Dalton Trans. (Camb. Engl. 2003) (2004) 2142–2151.
[59] Craig F. Bohren, Huffman, R. Donald, Absorption and Scattering of Light by Small Particles, Wiley, New York, 2013.
[60] A. Bedidi, B. Cervelle, J. Geophys. Res. 98 (1993) 11941–11952.
[61] H. Maeda, Y. Maeda, Langmuir ACS J. Surf. Colloids 27 (2011) 2895–2903.
[62] EU, Critical Raw Materials Resilience: Charting a Path towards greater Security and Sustainability, available at: ⟨https://eur-lex.europa.eu/legal-content/EN/TXT/PDF/?uri=CELEX:52020DC0474⟩.